Preparation and properties of extrusion-based 3D-printed hardmetal and cermet parts

Walter Lengauer[1], Ivica Duretek[2], Viktoria Schwarz[1], Christian Kukla[3], Michael Kitzmantel[4], Erich Neubauer[4], Clemens Lieberwirth[5], Vincent Morrison[5]

[1]Vienna University of Technology, Getreidemarkt 9/164CT, A-1060 Vienna
walter.lengauer@tuwien.ac.at viktoria.schwarz@tuwien.ac.at
[2]Montanuniversität Leoben, Dept. of Polymer Engineering Science, Otto-Glöckel-Str.2, A-8700 Leoben
ivica.duretek@unileoben.ac.at
[3]Montanuniversität Leoben, Industrial Liaison Dept., Peter-Tunner-Str. 27, A-8700 Leoben
christian.kukla@unileoben.ac.at
[4]RHP-Technology GmbH, A-2444 Seibersdorf
michael.kitzmantel@rhp-technology.com erich.neubauer@rhp-technology.com
[5]AIM3D GmbH, D-18069 Rostock
clemens.lieberwirth@aim3d.de vincent.morrison@aim3d.de

Abstract
Hardmetal and cermet bodies were printed by fused-filament fabrication (FFF) and composite-extrusion modelling (CEM) in an SDS (shaping – debinding – sintering) process. For FFF the filaments were prepared from hardmetal (WC-10Co) and cermet powder (Ti(C,N)-Co/Ni-based) and organic binder. The CEM feedstock consisted of WC-Co MIM powder. A 3D filament printer as well as a 3D printer working with a granulate such as used in MIM were employed to fabricate printed bodies by FFF and CEM, respectively. The solvent debinding process was performed in cyclohexane (FFF-printed bodies) or water (CEM-printed bodies). Thermal debinding of all parts was performed in a tube furnace up to a temperature of 800 °C. The pre-sintered parts were then subjected to vacuum sintering by application of conventional vacuum sintering profiles up to 1430 °C for hardmetals and up to 1460 °C for cermets. Dimensional and mass changes upon the various preparation steps as well as microstructure and porosity of the sintered bodies were investigated. While the microstructure is practically identical to that of conventionally prepared materials, some cavities are present from the printing process because of yet non-optimised printing strategy. The study shows that with the applied 3D printing techniques, hardmetal and cermet parts with innovative geometries are accessible.

1 Introduction

Additive manufacturing (AM) is a fast-developing technology in the field of powder metallurgy. Very complicated part geometries in combination with reduction in raw-powder consumption are the main benefits.
A low cost and very popular AM technique is the extrusion-based printing technology such as fused-filament printing. Since more than twenty years [1-3] feedstocks containing metal powders and various types of ceramic powders are being developed and plenty of studies appeared in the meantime. Contrary to the metal and ceramic powders studied so far, hardmetal and cermet formulations are mixtures of many different powders of grain sizes often smaller than 1 µm.
For 3D manufacturing of hardmetal and cermet bodies extrusion-based techniques are very interesting because of several advantages over other AM fabrication routes:

1) There is practically no raw material loss of extrusion-based methods. This is a benefit in view of the expensive hardmetal and cermet powder mixtures.
2) Hardmetal and cermet powder mixtures contain many different powders such as hard-phase powders (WC, Ti(C,N), VC, Cr_3C_2…) and binder powders (Co, Fe, Ni) which can separate if unbound powders incur in the shaping process (e.g. compare to powder-bed laser sintering). Such powders are difficult to recycle for re-use in the printing process.
3) Generally, hardmetal and cermets must have a uniform microstructure. Because of the presence of volatile Co, an SDS method (shaping - debinding - sintering) is a first choice. The whole part is sintered and no local overheating or unequal temperature distribution occurs which would result in binder loss and inhomogeneities in composition and grain size.
4) Extrusion-based techniques are the best-suited AM techniques for printing materials' combinations.

For the preparation of hardmetal and cermets we have studied here two extrusion-based methods, 1) the fused-filament fabrication (FFF) for which a feedstock filament was prepared and fed into a 3D printer and 2) composite-extrusion modelling (CEM) which can use MIM feedstock without need to prepare a filament. In both techniques the feedstock is fused and free-form printed through a nozzle. Our work seems to be the first study of FFF and CEM printing of hardmetals and cermets.

2 Experimental

2.1 Filament preparation

Filament Feedstock

For feedstock preparation, two powder batches, one hardmetal (WC-10%Co) and one cermet (Ti(C,N), WC, (Ta,Nb)C, Cr_3C_2, Co, Ni) batch (each approx. 1 kg) was prepared by ball mixing the starting powders in a 3 L polyurethane drum by use of hardmetal balls under cyclohexane for 24 h with an appropriate rotation speed to break agglomerates. After this procedure, the mixtures were dried in a vacuum oven.

The binder system for printing these inorganic powders had two components [4,5]: the main binder component and the backbone polymer. The main binder component was a soft and flexible thermoplastic elastomer – TPE (Kraiburg TPE GmbH & Co. KG, Germany). For the backbone, PP functionalized with maleic anhydride (BYK Chemie GmbH, Germany) was used. Some information of the prepared feedstocks is shown in Tab.1.

Feedstock	Main binder	Backbone	Backbone content in binder (vol%)	Powder content (vol%)
WC-Co	TPE	PP	40	50
Cermet				

Tab.1
Description of FFF feedstock materials.

Feedstocks were compounded in a kneader with counter rotating rollers (Plasti-Corder PL 2000, Brabender GmbH & Co. KG, Germany) at a rotational speed of 60 rpm. All the feedstock components were premixed in solid state. The kneader temperature was 200 °C and the total kneading time was 50 min. After compounding, the feedstocks were ground in a cutting mill (SM200, Retsch GmbH, Germany) with a sieve with square perforations of 4 mm in length.

Filament preparation

Filaments were prepared using a high-pressure capillary rheometer (Rheograph 2002, Göttfert Werkstoff-Prüfmaschinen GmbH, Germany). A round capillary with a diameter of 1.75 mm and length of 30 mm was used. Extrusion temperature was set at 200 °C and the piston speed was 1 $mm.s^{-1}$. The apparent shear rate was 215 s^{-1}. At the exit of the die, a Teflon conveyor belt was placed to pull the filament as it was extruded.

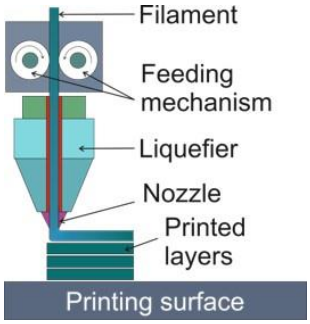

Fig.1
Scheme of the FFF technique.

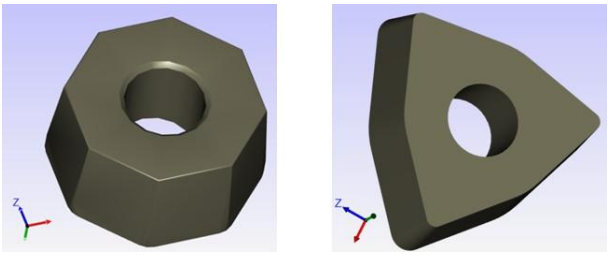

Fig.2
CAD drawing of printed indexable inserts.

Fused-filament fabrication (FFF)

Printing trials were performed on a Wanhao Duplicator i3V2 FFF with a nozzle diameter of 0.6 mm. A scheme of the FFF technique is shown in Fig.1. The printed parts were indexable cutting inserts with various geometries. The software KISSlicer was used to prepare the G-code for printing. Fig.2 shows a CAD drawing of parts printed by FFF.

In order to observe the powder wetting the filaments were investigated by means of scanning electron microscopy (SEM). The filaments were cryogenically fractured under liquid nitrogen.

2.2 Composite-extrusion modelling (CEM)

Another series of samples was fabricated by CEM-printing green bodies [6,7] from a hardmetal granulate used for MIM (PolyMIM, Bad Sobernheim, Germany). An ExAM 255 printer (AIM3D GmbH) with an

extruder heated to 190 °C was used. A scheme of this method is shown in Fig.3. After CAD modelling the program of Simplify 3D Inc. (Blue Ash, USA) was used to create printer and extruder commands. Printing was performed with a 0.3 mm nozzle and a layer height of 0.1 mm. The bed temperature was 100 °C. Printing time was between 15 and 20 min, depending on the part size.

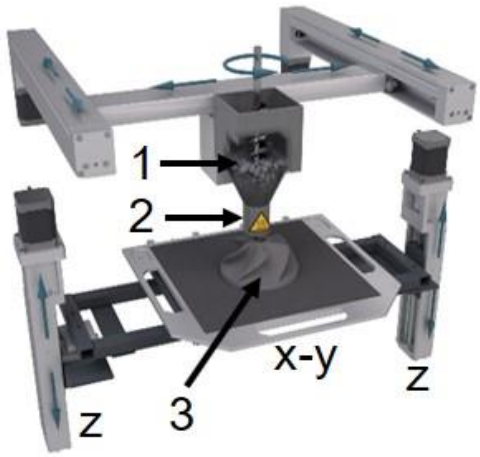

Fig.3
Scheme of the CEM technique, 1: pellet container, 2: extruder, 3: printed part, x-y: movable x-y table, z: movable z axis.

2.3 Debinding processes

Solvent debinding
FFF-printed parts of hardmetals and cermets were debound in cyclohexane at 60 °C for 48 h. All parts were dried at 70 °C in a vacuum oven.
CEM-printed green hardmetal bodies from PolyMIM feedstock were water debound by use of a mixture of H_2O with 2% inhibitor (Metamax I-15, Zschimmer & Schwarz, Germany) at 60 °C for 48 h.

Thermal debinding – pre-sintering
All parts were thermally debound in a tube furnace under flowing H_2 with a temperature ramp of 10 h to a maximum temperature of 800 °C.

2.4 Sintering and characterisation

After thermal debinding the bodies were subjected to vacuum sintering. Hardmetals were sintered within a simple time-temperature profile with a dwell at 1150 °C and at 1430 °C. A more complicated temperature profile was applied to cermets with three temperature dwells and a maximum sintering temperature of 1460 °C [8].
The parts were cut, diamond polished and inspected by light-optical (LOM) and scanning electron (SEM) microscopy.

3 Results and discussion

3.1 Filament quality

A constant geometry of the filament is important for its continuous transportation in an FFF machine. For this reason, the diameter and the ovality of the produced filament were monitored during production. The ovality distribution was more or less constant with an average of ±0.030 mm, which is sufficiently low to consider the filament to be round.Fig.4 shows SEM images where the good compatibility between the particles and the binder can be seen, since there are no gaps between the binder and the individual particles. One can see that the powder particles are equally distributed in the filament, which is important to have an even distribution of particles in the printed and sintered parts.

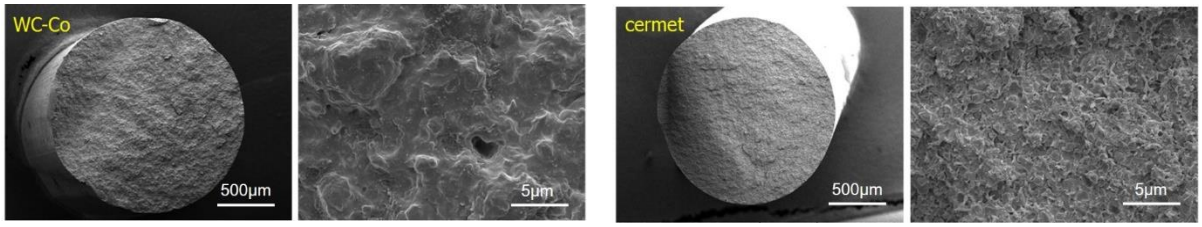

Fig.4
Overall view and detail of the filament filled with powder particles (left: hardmetal, right: cermet).

3.2 FFF-printed parts

In all printed parts the first layer had a good contact with the printing bed (Fig.5). The layer in contact with the printing bed had a more or less smooth and continuous surface (Fig.6). The printed layers were bonded correctly (Fig.7). Some defects can also be observed as a result of errors occurred during printing, for example small voids between the layers.

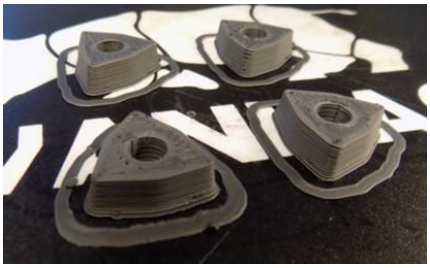

Fig.5
FFF printed parts on the printing bed.

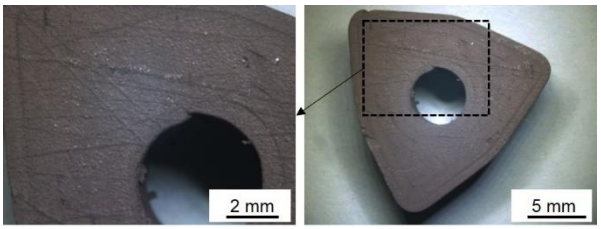

Fig.6
Bottom surface of FFF printed parts in contact with the bed.

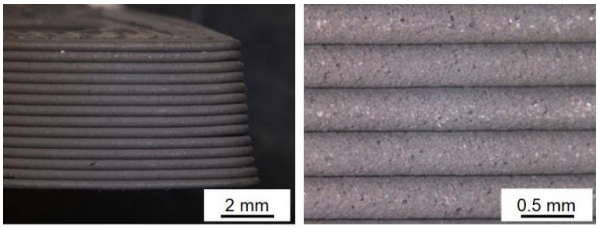

Fig.7
Layers of FFF printed parts.

3.3 Comparison of printed and sintered parts

Fig.8 shows a comparison between green and sintered FFF- and CEM-printed parts of hardmetals and cermets with a geometry similar to that of indexable inserts applied in metal cutting processes (turning and milling).

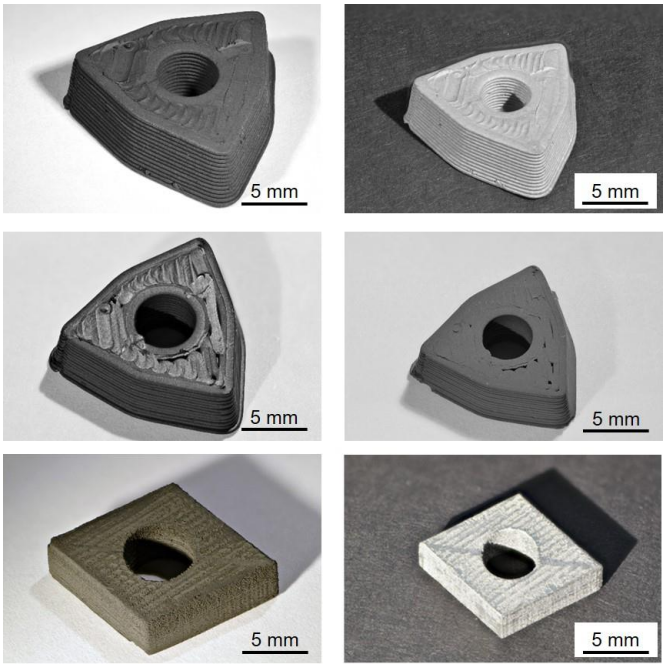

Fig.8
Printed and sintered bodies. Top row: FFF-printed (left) and sintered (right) hardmetal, middle row: FFF-printed (left) and sintered (right) cermet, bottom row: CEM-printed (left) and sintered (right) hardmetal.

The printing lines which are clearly visible in the green bodies (Fig.8, left column), prevail in the sintered parts (Fig.8, right column). This is also true for fine details and printing errors.

3.4 Mass change and geometries

Tab.2 gives details on mass change upon the various processing steps. After solvent debinding only the backbone remains in the body which serves for mechanical stability upon handling. Because of the substantially different density of hardmetals (ca. 15 $g.cm^{-3}$) and cermets (ca. 6.5 $g.cm^{-3}$) the mass loss of the latter is much higher.

Method	Part	Δm, % solvent debinding	Δm, % thermal debinding	Δm, % total, after sintering
FFF	Hardmetal	-3.55	-2.77	-6.31
FFF	Cermet	-7.08	-6.71	-14.62
CEM	Hardmetal	-3.40	-4.26	-7.82

Tab.2
Mass change after the various steps relative to the mass of printed body.

Tab.3 gives details on the dimensional changes. These have been determined by measuring the parts parallel and perpendicular to the printing plane.

Method	Part	Shrinkage x-y %	Shrinkage z %	Theoretical %
FFF	Hardmetal (coarse WC powder)	21.0	22.0	20.6
FFF	Cermet	21.6	22.3	20.6
CEM	Hardmetal (fine WC powder)	22.6	23.4	23.1

Tab.3
Dimensional changes before (3D-printed body) and after sintering. Theoretical shrinkage of FFF parts from powder/binder ratio, for CEM parts from PolyMIM data sheet.

For all parts the shrinkage in z direction is larger than in x-y direction. This is a consequence of denser packing density in x-y direction. Obviously, the printed lines within one layer are fused closer together than the one layer to the next. This could be due to solidification of the x-y printed layer before the next one is printed.

3.5 Microstructure and properties of sintered bodies

Fig.9 shows examples of the microstructure of an FFF-printed coarse-grained hardmetal. In Fig.9a and b cavities are visible which are aligned in the z direction (vertical). These cavities are due to some misalignment in x-y positioning upon printing so that a wedge-type gaps exist between the fused deposited filament lines within one layer. Similar observations of occurring cavities were reported on FFF-printed 361L steel parts [9]. The SEM image in Fig.9c shows the typical microstructure of hardmetals.
In Fig.10 microstructures of CEM-printed parts of fine-grained hardmetals are shown. These parts were fabricated with a finer nozzle than the FFF-printed parts. The cavities in z direction are more frequent but smaller. Here, another type of porosity is identified along x-y direction. These pores are quite small and are separated in z direction by the width of the fused filaments diameter. They stem from incomplete fusing of the fresh and liquid top line with the bottom plane composed of already solidified lines.
The SEM image of higher magnification (Fig.10c) shows again the typical hardmetal microstructure. Both hardmetal microstructures are quite uniform such as known from hardmetals fabricated by conventional processing techniques. They are located in the two-phase region WC-Co and do not show any eta phases (if carbon loss had occurred) or free C, which could be formed by carbon uptake upon thermal de-bindering from cracked organics.
Similar observations than with FFF-printed hardmetals were made for cermet printed parts (Fig.11). Again, there is mainly the cavities from misalignment in x-y direction (Fig.11a) because optimisation of printing strategy was not yet performed. Hardly any fine porosity from the sequence in the layer in z direction is observed. The SEM microstructure (Fig.11) shows the typical core-rime type character of hard-phase grains [10] not deviating from a conventionally fabricated cermet.

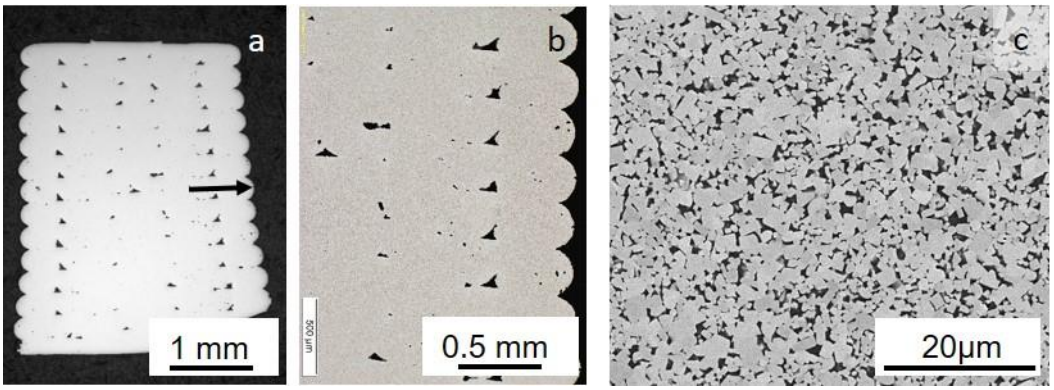

Fig.9
Cross sections (LOM) and microstructures (SEM) of FFF-printed coarse-grained WC-Co hardmetal. a: one half of the sample shown in Fig.8, top (arrow: inner wall); b: magnification of a (Murakami etched), f: SEM microstructure.

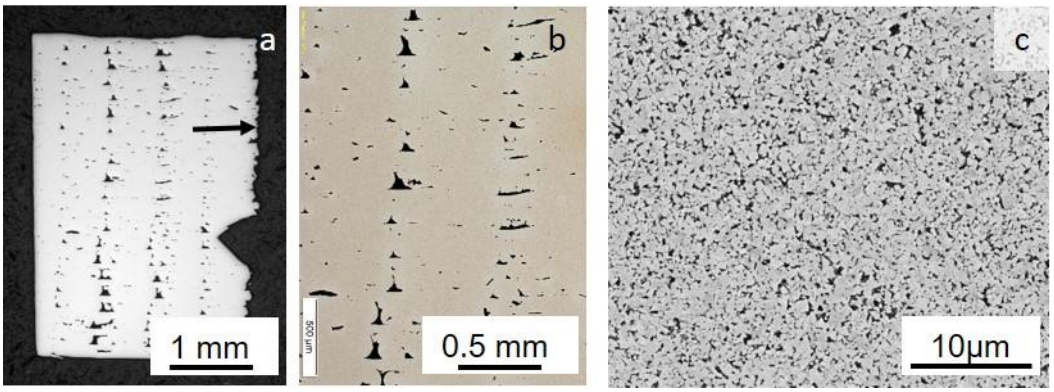

Fig.10
Cross sections (LOM) and microstructures (SEM) of CEM-printed fine-grained WC-Co hardmetal. a: one half of the sample in Fig.8, bottom (arrow: inner wall); b: magnification of a (Murakami etched), c: SEM microstructure.

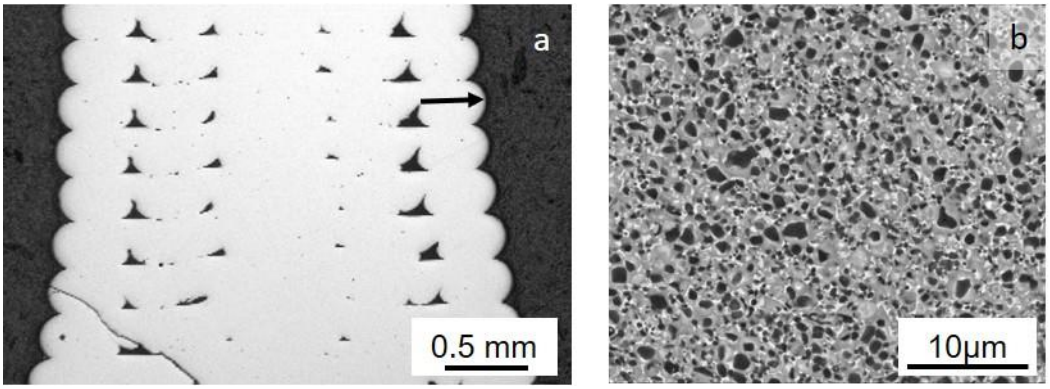

Fig.11
Cross sections (LOM) and microstructure (SEM) of an FFF-printed Ti(C,N)-based cermet. (a) one half of the part shown in Fig.8, centre (arrow: inner wall); (b) SEM microstructure.

3.6 Modifications

3D printing techniques cover the potential of fabricating geometrical details which are not accessible by other techniques. In case of the above-presented parts which are related to indexable inserts for metal cutting applications this means that hollow parts could be fabricated which can save material consumption or which cover cooling channels. Fig.12 shows such a printed insert (with W-type geometry) with a central hole and three cooling channels near the tips.

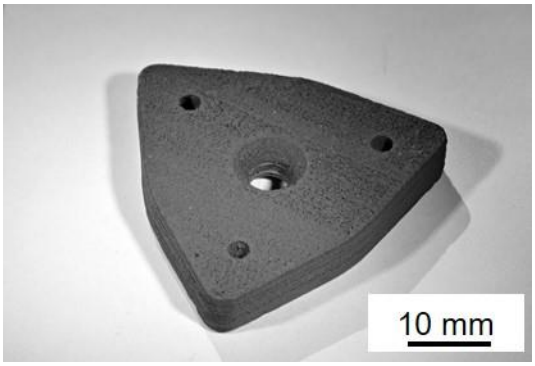

Fig.12
A prototype of a CEM-printed indexable insert (WC-Co hardmetal) with cooling channels.

At the present stage of printer technology the nozzles have a diameter of ca. 0.3 – 0.6 mm. This is too large if very fine structures and reliefs are to be manufactured. One solution of making fine structures is the post-processing of the green printed parts. This is easy as these parts contain about 50 vol% organic material and hence simple grinding, blasting and mechanical machining is possible and inexpensive. Other methods could be laser surface treatment [9] or gas-phase treatment with solvents to smoothen the surface is another possibility. In this work we have investigated a simple imprinting for surface conditioning.
Fig.13 shows an FFF-printed part (after printing and after sintering) into which a relief was imprinted simply by pressing a hot counterpart (of defined temperature for a defined time) onto the surface of the printed green body.

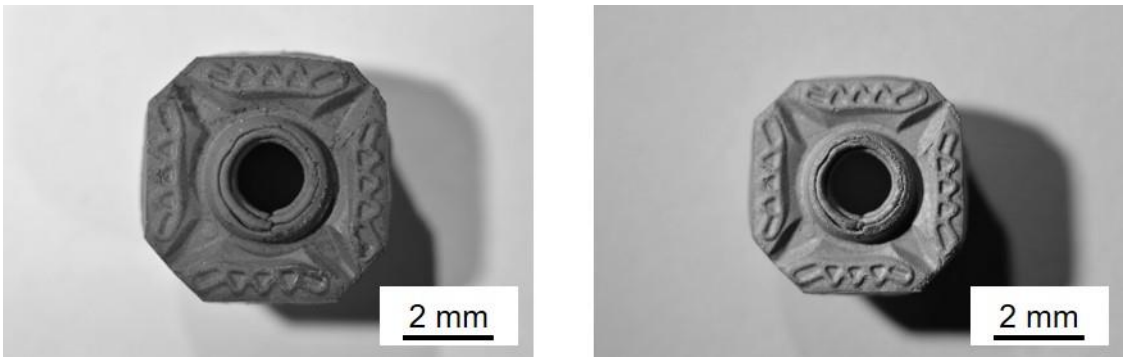

Fig.13
Printed parts with an imprint of an indexable insert, (a) green part, (b) sintered part.

The results show that even very fine structures of the green body persist the whole preparation process and are present in the sintered part. Such an imprinting, together with other techniques mentioned above, can circumvent the present lack of accuracy of extrusion-based printed bodies. A cross section of the part shown in Fig.13 is given in Fig.14.
The surface does not show any cavities from the misalignment of deposited lines in x-y direction but some inner cavities are enlarged due to the impact of static load.

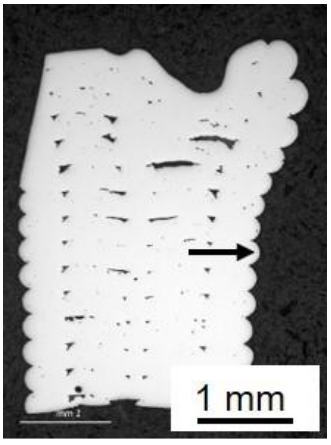

Fig.14
Cross section (LOM) of one half of the part shown in Fig.11 (arrow: inner wall) with an imprint of a hot counterpart on top.

4 Conclusion

In this study we have shown that extrusion-based 3D printing by FFF and CEM is possible by employing powder mixtures of hardmetals and cermets. Parts of these materials were sintered and showed the typical microstructures. Complete density was not yet achieved because the printing strategy was not yet optimised and cavities occur from the printing process. Hence, the organic binder system together with the printing procedure and hardware (printer nozzles) need to be further optimised. However, our work is the first study on extrusion-based 3D printing of hardmetal and cermet parts by CEM (composite-extrusion modelling) and FFF (fused filament fabrication) and is was proven that these printing techniques are well-suited for an SDS (shaping – debinding – sintering) type of part fabrication. By further development of this technology hardmetal and cermet parts with complicated geometries and new properties not accessible by other techniques can be expected.

References

[1] M.K.Agarwala, Structural ceramics by fused deposition of ceramics, *Proc. Solid Freeform Fabrication Symposium*, p.1-8 (1995)

[2] M.A.Yardimci, S.I.Guceri, S.C.Danforth, Process modelling for fused deposition of ceramics, *Ceram.Engineer.Sci.Proc.* 17(3), 78-82 (1996)

[3] G.Wu et al. Fabrication of Metal Components using FDMet: Fused Deposition of Metals, *Proc. Solid Freeform Fabrication Symposium* 1996, p.775-782 (1996)

[4] C.Kukla, I.Duretek, S.Schuschnigg, J. Gonzalez-Gutierrez, C.Holzer, Properties for PIM Feedstocks Used in Fused Filament Fabrication, *Proc. WorldPM* (2016)

[5] C.Kukla, J.Gonzalez-Gutierrez, C.Burkhardt, C.Holzer, The production of Magnets by FFF – Fused Filament Fabrication, *Proc. EuroPM* (2017)

[6] C.Lieberwirth, A.Harder, H.Seitz, Additive manufacturing with metal injection molding granules, *Rapid. Tech.- Intl. Trade Show & Conf. for Additive Manufacturing* (2016)

[7] C.Lieberwirth, A.Harder, H.Seitz, Extrusion Based Additive Manufacturing of Metal Parts, *J.Mech.Engineer. Autom.* 7, 79-83 (2017)

[8] A.Demoly, C.Veitsch, W.Lengauer, K.Rabitsch, Effect of submicron Ti(C,N) on the microstructure and the mechanical properties of Ti(C,N)-based cermets, *Int.J.Refr.Met.&Hard Mater.* 29(6), 716-723 (2011)

[9] C.Burkhardt, P.Freigassner, O.Weber, P.Imgrund, S.Hampel, Fused filament fabrication (FFF) of 316L Green Parts for the MIM process, *Proc. WorldPM* (2016)

[10] P.Ettmayer, H.Kolaska, W.Lengauer, K.Dreyer, Ti(C,N)-based Cermets – Metallurgy and Properties, *Int.J.Refr.Met.&Hard Mater.* 13, 343-351 (1995)